Broadband photoresponse of graphene photodetector from visible to long-wavelength infrared wavelengths

Shinpei Ogawa
Masaaki Shimatani
Shoichiro Fukushima
Satoshi Okuda
Yasushi Kanai
Takao Ono
Kazuhiko Matsumoto

Broadband photoresponse of graphene photodetector from visible to long-wavelength infrared wavelengths

Shinpei Ogawa,[a,*] Masaaki Shimatani,[a] Shoichiro Fukushima,[a] Satoshi Okuda,[a] Yasushi Kanai,[b] Takao Ono,[b] and Kazuhiko Matsumoto[b]

[a]Advanced Technology R&D Center, Mitsubishi Electric Corporation, Amagasaki, Japan
[b]Osaka University, Institute of Scientific and Industrial Research, Osaka, Japan

Abstract. Graphene-based transistors were investigated as simple photodetectors for a broad range of wavelengths. Graphene transistors were prepared using p-doped silicon (Si) substrates with a SiO$_2$ layer, and source and drain electrodes. Monolayer graphene was fabricated by chemical vapor deposition and transferred onto the substrates, and the graphene channel region was then formed. The photoresponse was measured in the broadband wavelength range from the visible, near-infrared (NIR), and mid- to long-wavelength IR (MWIR to LWIR) regions. The photoresponse was enhanced by the photogating induced by the Si substrate at visible wavelengths. Enhancement by the thermal effect of the insulator layer became dominant in the LWIR region, which indicates that the photoresponse of graphene-based transistors can be controlled by the surrounding materials, depending on the operation wavelength. These results are expected to contribute to provide the key mechanism of high-performance graphene-based photodetectors. © *The Authors. Published by SPIE under a Creative Commons Attribution 4.0 Unported License. Distribution or reproduction of this work in whole or in part requires full attribution of the original publication, including its DOI.* [DOI: 10.1117/1.OE.58.5.057106]

Keywords: graphene; photodetectors; broadband; photogating.

Paper 190270 received Feb. 27, 2019; accepted for publication May 8, 2019; published online May 29, 2019.

1 Introduction

Graphene is a single atomic layer of carbon with a hexagonal lattice, which results in a unique bandgap structure as Dirac cones.[1] Such structures produce exciting optoelectronic properties, such as fast electron mobility and broadband absorption that ranges from at least the ultraviolet region to the terahertz region.[2] Many applications are expected for these structures, such as transistors,[3] photodetectors,[4] biological sensors,[5] and supercapacitors.[6] Other two-dimensional materials have also been applied to photodetectors.[7,8] In particular, black phosphorus[9,10] has been widely studied for infrared (IR) detector applications due to its bandgap in the middle wavelength IR (MWIR) region. However, the instability of black phosphorus is a serious disadvantage. Therefore, graphene is a strong candidate for photodetector materials because it satisfies numerous demands—broadband photoresponse from the ultraviolet to terahertz regions, high-speed operation, stability, and low fabrication costs—which have not been simultaneously achieved with the current technology. The main disadvantage of graphene is lack of bandgap, which leads to high dark current. However, this can be overcome by using graphene nanoribbons.[11,12] Therefore, we have investigated graphene as an advanced material with an aim to realize photodetectors based on a new concept. However, the poor absorption of graphene, at about 2.3%, still remains an important issue to address.

Graphene-based transistors are being investigated as simple photodetectors for various wavelength regions. Most research has focused on enhancement of the responsivity using various methods, such as p-n junctions,[13,14] plasmonic resonance,[15,16] asymmetric electrodes,[17,18] optical cavities,[19] waveguides,[20,21] nanoribbons,[8,22] and optical gating.[23–27] However, although graphene is highly sensitive to the surrounding materials and its influence changes according to the wavelength, the photoresponse mechanism in the broadband wavelength region from visible to long-wavelength IR (LWIR) has been less studied.[28] In particular, the materials surrounding graphene have a strong effect on its optical properties.[24,25] It is thus important to investigate the effects of these materials experimentally to reveal the photoresponse mechanism of graphene photodetectors. We have previously investigated the influence of the surrounding materials for broadband photoresponse;[29] however, no direct evidence of the photogating induced by the substrate from the visible to LWIR wavelengths was demonstrated. Here, we report the detailed mechanism that defines the photoresponse of graphene-based transistors with respect to various factors, such as the operation wavelength, the components near the graphene channel in the photodetector, and the temperature.

2 Device Structures and Fabrication

Figure 1(a) shows schematic illustrations of the graphene photodetector, which is based on a graphene field-effect transistor (G-FET). A p-type silicon (Si) substrate was first prepared with a 290-nm-thick thermal oxide (SiO$_2$) layer. Then, 10-nm/30-nm-thick Cr/Au-based source and drain electrodes were formed on the substrate by a lift-off technique. Monolayer graphene was fabricated by chemical vapor deposition (CVD) and then transferred onto the substrate with the source and drain electrodes using the conventional graphene-transfer method.[30] The graphene channel was then formed by photolithography and O$_2$ etching. The graphene channel length and width were 20 and 10 μm, respectively. Figure 1(b) shows an optical microscopy image of the developed graphene photodetector, and Fig. 1(c) shows a Raman

*Address all correspondence to Shinpei Ogawa, E-mail: Ogawa.Shimpei@eb.MitsubishiElectric.co.jp
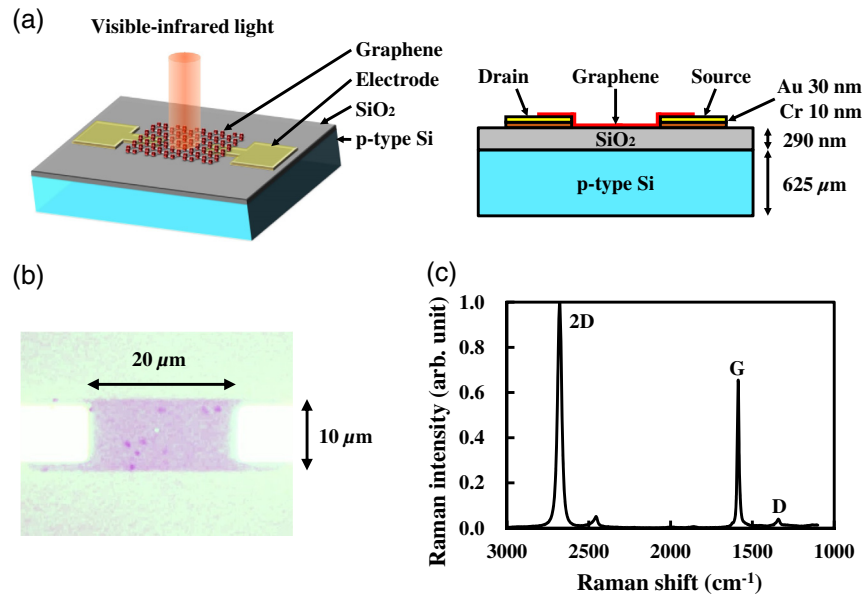
(a)

Visible-infrared light

Graphene
Electrode
SiO₂
p-type Si

Drain   Graphene   Source

Au 30 nm
Cr 10 nm
SiO₂
290 nm
p-type Si
625 μm

(b)

20 μm

10 μm

(c)

Fig. 1 (a) Schematic illustration, (b) optical microscopy image, and (c) Raman spectrum of the developed graphene photodetector.

spectrum confirming that the monolayer graphene channel was successfully formed without obvious defects.[31]

3 Measurement and Results

The photoresponse of the developed graphene photodetector was measured. The Dirac point of the graphene photodetector was tuned to a back-gate voltage (V_{bg}) of about 0 V using vacuum annealing. Figure 2 shows a schematic illustration of the measurement system with a photograph of the graphene photodetector placed in the measurement system. The developed graphene photodetectors have no polarization dependence because graphene is isotropic. The graphene photodetector was set in the vacuum probe system with a cooler. Diode lasers (DLs) were used as visible light source with wavelengths at 0.6 μm and near-IR (NIR) light at 1.6 μm, and a quantum cascade laser (QCL) was used MWIR light at 4.6 μm and LWIR light at 7.9 and 9.6 μm. All light sources were operated in pulse mode. The pulse duration and ratio are 1.2 s and 0.5 Hz for the wavelengths
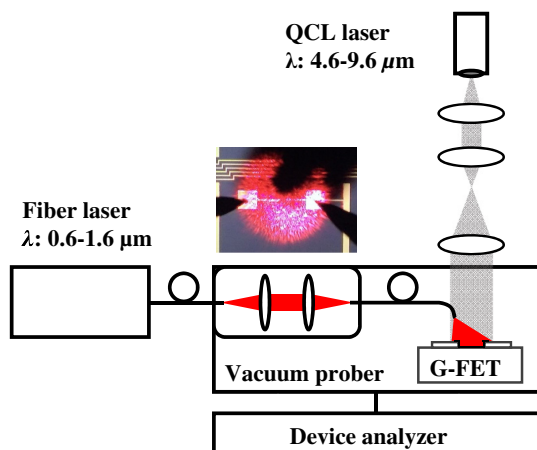
QCL laser
λ: 4.6-9.6 μm

Fiber laser
λ: 0.6-1.6 μm

Vacuum prober   G-FET

Device analyzer

Fig. 2 Schematic illustration of the measurement system with photograph of the illuminated G-FET in the measurement system.

of 0.6 and 1.6 μm, and 1.0 s and 0.5 Hz for the wavelengths of 4.6, 7.9, and 9.6 μm, respectively. The source-drain bias voltage (V_{sd}) was 0.1 V. V_{bg} was applied to the back side of the Si substrate and was varied from −50 to 50 V, from which the maximum responsivity was determined.

Figures 3(a)–3(e) show the time-dependent photocurrent (I_{ph}) of the graphene photodetector at wavelengths of 0.6, 1.6, 4.6, 7.9, and 9.6 μm, respectively. The same V_{sd} and V_{bg} of 0.1 and 0 V were used for each wavelength. I_{ph} was calculated from the source-drain current (I_{sd}) difference between the illuminated and dark conditions. The dark current was ~10 μA for all wavelengths. The measurement temperature was room temperature (RT) for 0.6 μm and 14 K for 1.6, 4.6, 7.9, and 9.6 μm. No optical response was obtained at RT for wavelengths of 1.6, 4.6, 7.9, and 9.6 μm, which is attributed to the thermal noise at IR wavelengths. The measurement at a wavelength of 0.6 μm was performed at a temperature of 14 K, and the responsivity was higher than that at RT. However, photodetector applications at visible wavelengths are typically carried out at RT. Therefore, we conducted our measurements for 0.6 μm at RT. It should be noted that the input power was different at each wavelength due to the performance of each light source. The input optical power was 0.606 pW, 1427 nW, 100.5 nW, 405.4 nW, and 165.1 nW for 0.6, 1.6, 4.6, 7.9, and 9.6 μm, respectively. The I_{ph} response was noisier in the IR wavelength regions, which was attributed to the noisy output pulse of the QCL used for this measurement.

Figures 3(a)–3(e) show that the broadband photoresponse was successfully obtained from the visible, NIR, MWIR, and LWIR regions, which is consistent with graphene theory. However, cooling was required for the IR wavelength regions.

Figures 4(a)–4(e) show the measured I_{ph} as a function of the input optical power for each wavelength. The other measured conditions are the same as in Fig. 3. Figures 4(a)–4(b) show that in the visible and NIR, the photoresponse was nonlinear and saturation was observed. Figures 4(c)–4(e) show
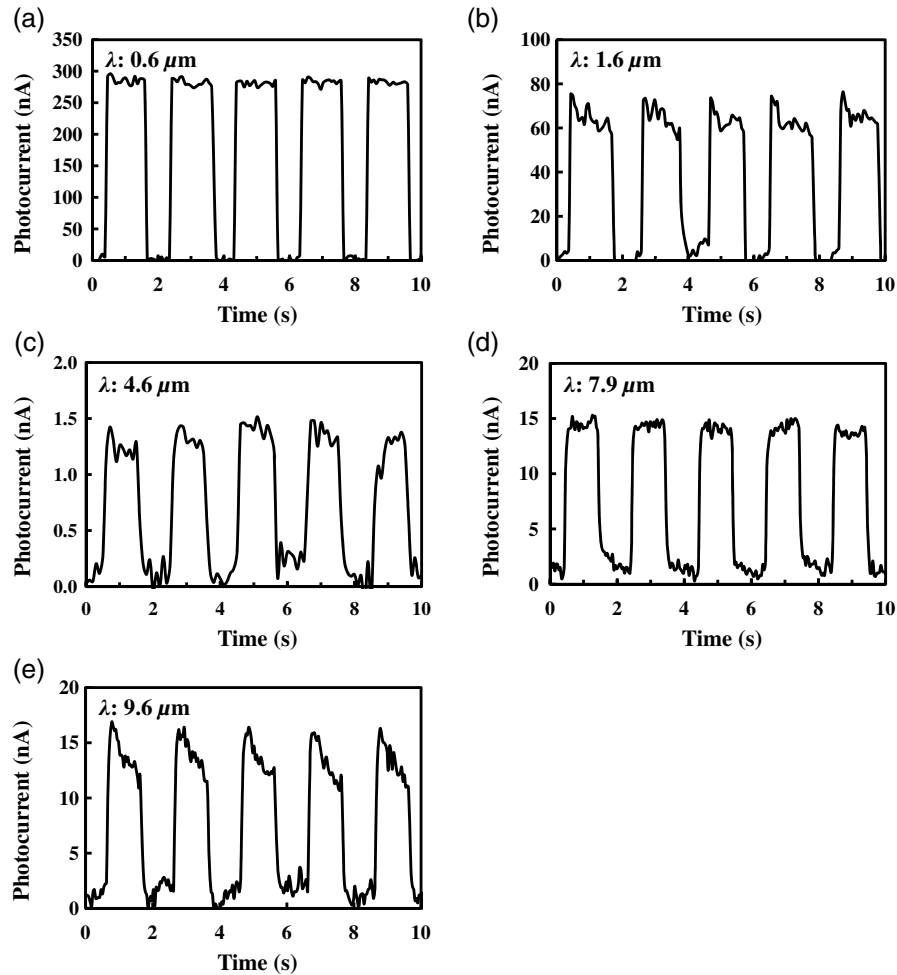
Fig. 3 Time-dependent photocurrent response at wavelengths of (a) 0.6, (b) 1.6, (c) 4.6, (d) 7.9, and (e) 9.6 μm.

that in the MWIR and LWIR, a linear photoresponse was obtained.

4 Discussion

The responsivity (A/W) of the graphene photodetector was calculated for each measured wavelength, and the results are given in Fig. 5. The responsivity in the visible and NIR was calculated for input optical powers smaller than 10 nW in order to clarify the photogating effect discussed later. The responsivity in the MWIR and LWIR was calculated from the slope of the I_{ph} versus input optical power curve.

Figure 5 shows two unique phenomena: (1) the responsivity in the visible wavelengths was so high that the quantum efficiency exceeded 100% at RT. (2) The responsivities in the LWIR region with wavelengths of 7.9 and 9.6 μm were larger than that in the MWIR region with a wavelength of 4.6 μm. The first phenomenon suggests that an effect other than photoelectric conversion occurred in the graphene photodetector.

The first phenomenon was investigated in detail. The V_{bg} and V_{sd} dependence of I_{ph} at wavelengths of 0.6 and 9.6 μm was measured to compare the photoresponse at the visible and IR wavelengths. Figures 6(a) and 6(b) show the measured V_{bg} dependence of I_{ph} with V_{sd} at 1.0 V and the V_{sd} dependence of I_{ph} with V_{bg} at 0 V for a wavelength

of 0.6 μm, respectively, while Figs. 6(c) and 6(d) show the same for a wavelength of 9.6 μm.

Figures 6(a) and 6(b) show that I_{ph} at the visible wavelength is strongly dependent on V_{bg} and is proportional to V_{sd}. In contrast, Figs. 6(c) and 6(d) show that I_{ph} at the IR wavelength is almost constant and is not dependent on V_{sd}. Figure 6(a) shows that I_{ph} at the visible wavelength is larger at negative V_{bg} than that at positive V_{bg}, which suggests that the substrate has some effect on this phenomenon. To investigate this difference in detail, we measured the gate current, which can be considered as the current that flows through the substrate, for both wavelengths. Figures 7(a) and 7(b) show the gate current with I_{ph} at wavelengths of 0.6 and 9.6 μm, respectively.

Figures 7(a) and 7(b) show that although the gate current in the visible wavelength was strongly induced by the incident light and affected I_{ph}, there was no obvious gate current in MWIR or LWIR region. Therefore, this phenomenon was mainly attributed to the generation of photocarriers in the Si substrate, which has a bandgap at a shorter wavelength of 1.1 μm. Note that high quantum efficiency was obtained at 1.6 μm due to the photogating effect caused by the impurity level to band absorption in the p-type Si substrate. This phenomenon was only observed at the low temperature of 14 K.
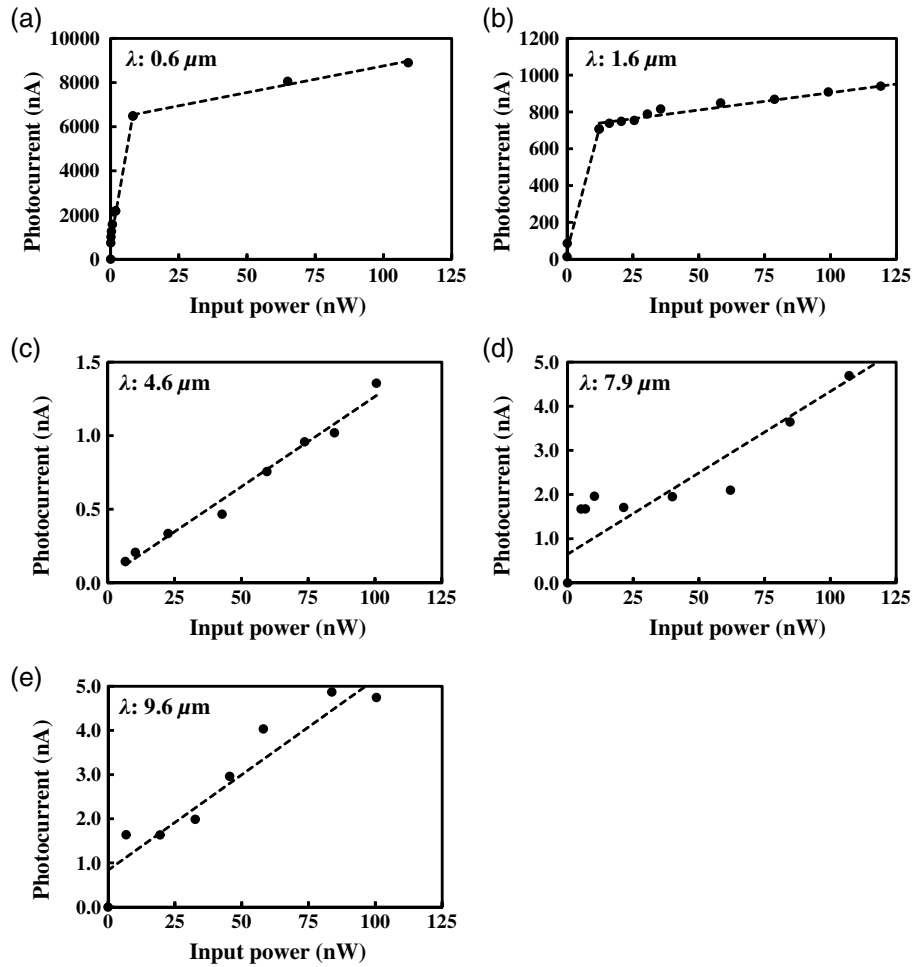
Fig. 4 Photocurrent response as a function of the input optical power at wavelengths of (a) 0.6, (b) 1.6, (c) 4.6, (d) 7.9, and (e) 9.6 μm.
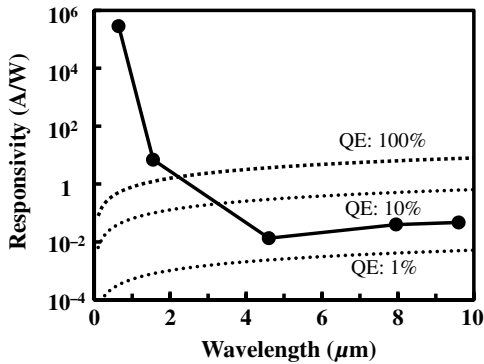

Fig. 5 Responsivity of the developed graphene photodetector for each wavelength.

Figure 8 shows this mechanism schematically. When negative V_{bg} was applied, the majority carriers (holes) are moved to the back gate and a depletion layer is formed between the interface of SiO_2 and Si. Photocarriers are then generated in this depletion layer by the incident light. These photocarriers slightly modulate V_{bg} for the graphene channel. The mobility of graphene is extremely fast and its thickness is one atomic layer; therefore, a slight change of the gate voltage can produce a giant change in I_{ph}, which is known as the photogating effect. The obtained change in I_{ph} is proportional to the product of the mobility and the change in the gate voltage.[26]

The photoelectric conversion of Si occurs at a shorter wavelength of 1.1 μm, which corresponds to the wavelength region where the extraordinarily high-responsivity region was observed in Fig. 4. Therefore, as shown in Fig. 6(a), high I_{ph} was obtained at negative V_{bg}, which formed the depletion region. In contrast, there is little photoelectric conversion at the IR wavelengths and no V_{bg} dependence as shown in Fig. 6(c). These results are direct evidence of the photogating effect due to the photocarrier generation in the Si substrate, which results in ultrahigh responsivity. It should be noted that IR measurements were performed at 14 K, so that very few photocarriers were generated due to the impurity level in the Si, and only a slight photogating effect was observed mainly in the NIR wavelength region.

The second phenomenon, the difference between the responsivity in the MWIR and LWIR regions, was investigated next, as shown in Fig. 5. A comparison of Figs. 6(b)–6(d) suggests that a different mechanism from that for a conventional phototransistor may occur at IR wavelengths. The responsivity in the LWIR region was slightly larger
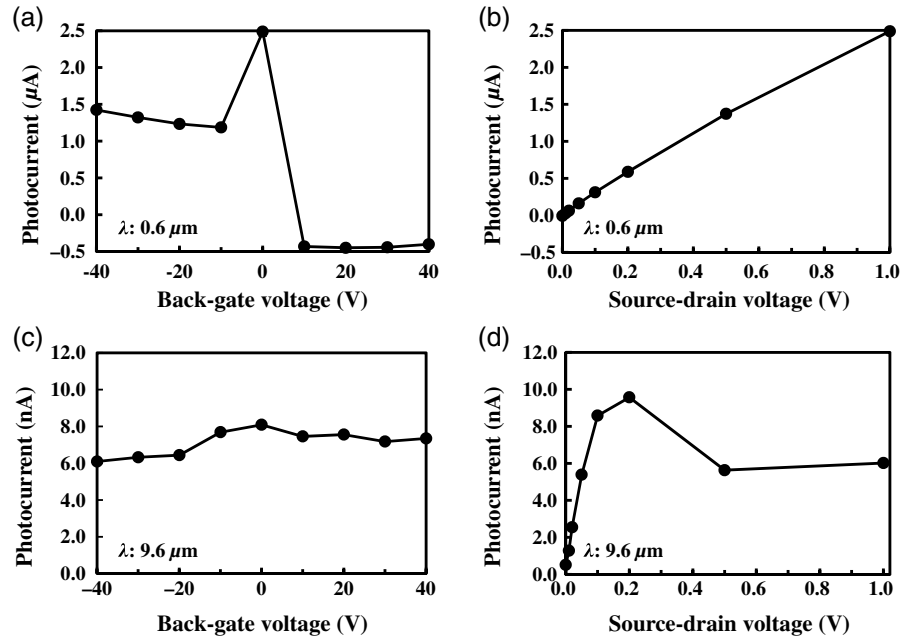
Fig. 6 I_{ph} as a function of (a) V_{bg} and (b) V_{sd} at a wavelength of 0.6 μm, and (c) V_{bg} and (d) V_{sd} at a wavelength of 9.6 μm.
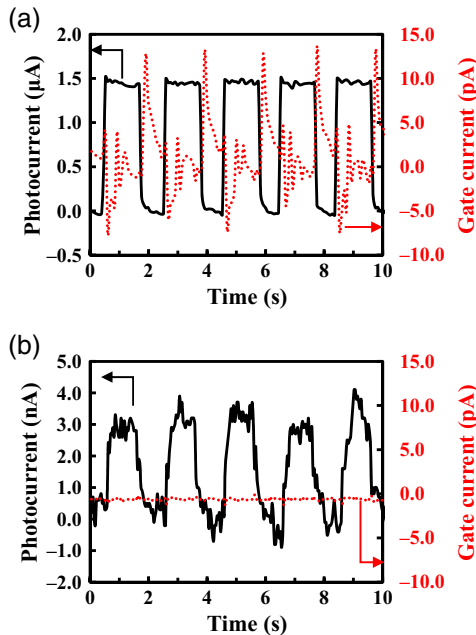

Fig. 7 Time-dependent I_{ph} and gate current at wavelengths of (a) 0.6 and (b) 9.6 μm.

Fig. 8 Schematic illustration of the photogating effect of the developed graphene photodetector at visible wavelengths.

than that for the MWIR region, despite the larger thermal noise. This may be due to absorption by the SiO$_2$ layer. The absorbance of SiO$_2$ for a Si substrate thickness of 290 nm was calculated using rigorous coupled-wave analysis and the material constant for SiO$_2$ taken from Ref. 32. Figure 9 shows the calculated results.

The absorbance of SiO$_2$ was more enhanced at a wavelength of 9.6 μm than at 4.6 and 7.9 μm, which corresponds to the responsivity difference shown in Fig. 5. Multiple reflections do not occur in this calculation model. Multiple
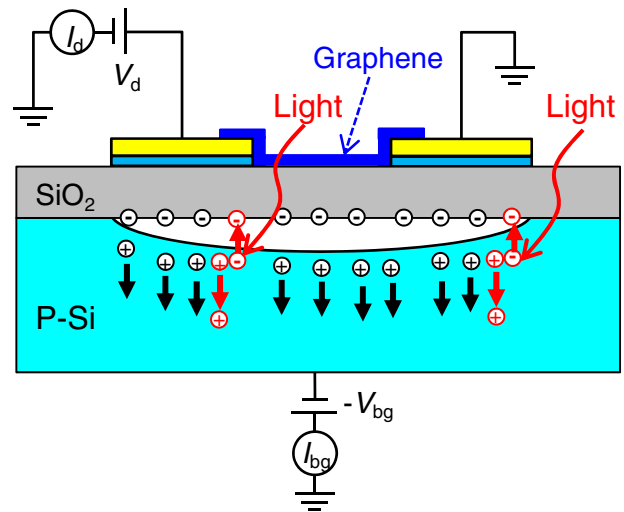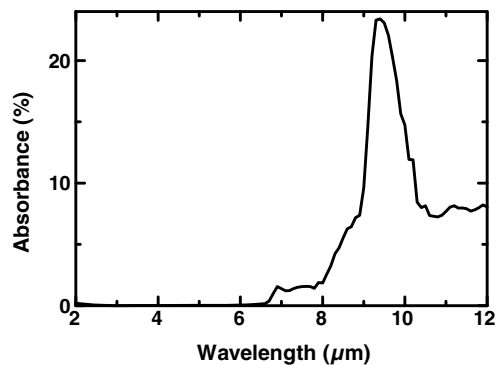

Fig. 9 Absorbance of SiO$_2$ for a Si substrate thickness of 290 nm.

reflections can occur by the back side of the substrate; therefore, more light could be absorbed than that indicated by the results of this calculation. This absorbed light was converted to heat, which induced a bolometric effect[33] in graphene and enhanced the responsivity in the LWIR region, which caused the difference of the responsivity between the MWIR and LWIR regions. The G-FET has a symmetric structure so that the thermoelectric effect[34,35] in graphene can be negligible compared to the bolometric effect. Graphene terahertz detectors using the thermoelectric effect induced by the asymmetry of contact metals have been developed.[36] Thus, the responsivity of graphene can be enhanced by the surrounding materials and the thermal effect of the insulator, depending on the operation wavelength.

5 Conclusion

An FET-based graphene photodetector was developed using a conventional graphene transfer technique. The photoresponse was measured in the visible, NIR, MWIR, and LWIR regions. The responsivity was calculated from the visible to LWIR wavelengths. Ultrahigh responsivity was obtained around the visible wavelength region. The V_{bg} and V_{sd} dependence of I_{ph} and the gate current were also measured to investigate this phenomenon. These results provided direct evidence of the photogating effect induced by the depletion layer between the Si substrate and the SiO_2 layer at visible wavelengths at RT, which correspond to the Si bandgap. Cooling was required at wavelengths longer than visible due to thermal noise. Enhancement by the bolometric effect of the insulator layer became dominant in the LWIR region, which indicates that the photoresponse of graphene-based transistors can be controlled by the surrounding materials, depending on the operation wavelength. For example, InSb[26] or a pyroelectric material such as $LiNbO_3$[27] as a substrate can enhance the responsivity in the MWIR or LWIR regions, respectively, because InSb has a bandgap in the MWIR and a pyroelectric material induces a voltage change due to the pyroelectric effect. The results of this study demonstrate that various graphene photoresponse mechanisms take place over the visible to LWIR wavelength regions. These mechanisms should be understood in order to further develop broadband operation. The photogating effect is a promising route to achieving ultrahigh responsivity, especially for low input optical powers, but it requires finding the appropriate materials for photogating and suppression of the graphene dark current by, for example, using graphene nanoribbons. These results are expected to contribute to the framework for development of high-performance graphene-based photodetectors.

References

1. A. H. Castro Neto et al., "The electronic properties of graphene," *Rev. Mod. Phys.* **81**(1), 109–162 (2009).
2. F. Bonaccorso et al., "Graphene photonics and optoelectronics," *Nat. Photonics* **4**, 611–622 (2010).
3. F. Schwierz, "Graphene transistors," *Nat. Nanotechnol.* **5**(7), 487–496 (2010).
4. F. H. L. Koppens et al., "Photodetectors based on graphene, other two-dimensional materials and hybrid systems," *Nat. Nanotechnol.* **9**(10), 780–793 (2014).
5. S. J. Heerema and C. Dekker, "Graphene nanodevices for DNA sequencing," *Nat. Nanotechnol.* **11**(2), 127–136 (2016).
6. D. Chen et al., "Graphene-like layered metal dichalcogenide/graphene composites: synthesis and applications in energy storage and conversion," *Mater. Today* **17**(4), 184–193 (2014).
7. Z. Sun and H. Chang, "Graphene and graphene-like two-dimensional materials in photodetection: mechanisms and methodology," *ACS Nano* **8**(5), 4133–4156 (2014).
8. S. C. Dhanabalan et al., "Present perspectives of broadband photodetectors based on nanobelts, nanoribbons, nanosheets and the emerging 2D materials," *Nanoscale* **8**(12), 6410–6434 (2016).
9. Q. Guo et al., "Black phosphorus mid-infrared photodetectors with high gain," *Nano Lett.* **16**(8), 4648–4655 (2016).
10. X. Ren et al., "Environmentally robust black phosphorus nanosheets in solution: application for self-powered photodetector," *Adv. Funct. Mater.* **27**(18), 1606834 (2017).
11. M. Freitag et al., "Photocurrent in graphene harnessed by tunable intrinsic plasmons," *Nat. Commun.* **4**, 1951 (2013).
12. A. Celis et al., "Graphene nanoribbons: fabrication, properties and devices," *J. Phys. D: Appl. Phys.* **49**(14), 143001 (2016).
13. N. Liu et al., "Large-area, transparent, and flexible infrared photodetector fabricated using P-N junctions formed by N-doping chemical vapor deposition grown graphene," *Nano Lett.* **14**(7), 3702–3708 (2014).
14. M. Shimatani et al., "Photocurrent enhancement of graphene phototransistors using p-n junction formed by conventional photolithography process," *Jpn. J. Appl. Phys.* **55**(11), 110307 (2016).
15. S. Ogawa, D. Fujisawa, and M. Ueno, "Effect of graphene on plasmonic metasurfaces at infrared wavelengths," *AIP Adv.* **3**(11), 112127 (2013).
16. S. Ogawa et al., "Graphene on metal-insulator-metal-based plasmonic metamaterials at infrared wavelengths," *Opt. Express* **26**(5), 5665 (2018).
17. T. Mueller, F. Xia, and P. Avouris, "Graphene photodetectors for high-speed optical communications," *Nat. Photonics* **4**(5), 297–301 (2010).
18. T. J. Yoo et al., "Zero-bias operation of CVD graphene photodetector with asymmetric metal contacts," *ACS Photonics* **5**(2), 365–370 (2017).
19. M. Furchi et al., "Microcavity-integrated graphene photodetector," *Nano Lett.* **12**(6), 2773–2777 (2012).
20. X. Gan et al., "Chip-integrated ultrafast graphene photodetector with high responsivity," *Nat. Photonics* **7**(11), 883–887 (2013).
21. X. Wang et al., "High-responsivity graphene/silicon-heterostructure waveguide photodetectors," *Nat. Photonics* **7**(11), 888–891 (2013).
22. X. Yu et al., "A high performance, visible to mid-infrared photodetector based on graphene nanoribbons passivated with HfO2," *Nanoscale* **8**(1), 327–332 (2016).
23. G. Konstantatos et al., "Hybrid graphene-quantum dot phototransistors with ultrahigh gain," *Nat. Nanotechnol.* **7**(6), 363–368 (2012).
24. M. Shimatani et al., "Giant Dirac point shift of graphene phototransistors by doped silicon substrate current," *AIP Adv.* **6**(3), 035113 (2016).
25. X. Guo et al., "High-performance graphene photodetector using interfacial gating," *Optica* **3**(10), 1066–1070 (2016).
26. S. Fukushima et al., "High responsivity middle-wavelength infrared graphene photodetectors using photo-gating," *Appl. Phys. Lett.* **113**(6), 061102 (2018).
27. M. Shimatani et al., "Enhanced photogating via pyroelectric effect induced by insulator layer for high-responsivity long-wavelength infrared graphene-based photodetectors operating at room temperature," *Appl. Phys. Exp.* **12**(2), 025001 (2019).
28. B. Y. Zhang et al., "Broadband high photoresponse from pure monolayer graphene photodetector," *Nat. Commun.* **4**, 1811 (2013).
29. S. Ogawa et al., "Broadband photoresponse of graphene photodetector from visible to long-wavelength infrared wavelengths," *Proc. SPIE* **10624**, 1062415 (2018).
30. J. W. Suk et al., "Transfer of CVD-grown monolayer graphene onto arbitrary substrates," *ACS Nano* **5**(9), 6916–6924 (2011).
31. D. Graf et al., "Spatially resolved Raman spectroscopy of single- and few-layer graphene," *Nano Lett.* **7**(2), 238–242 (2007).
32. R. Kitamura, L. Pilon, and M. Jonasz, "Optical constants of silica glass from extreme ultraviolet," *Appl. Opt.* **46**(33), 8118–8133 (2007).
33. J. Yan et al., "Dual-gated bilayer graphene hot-electron bolometer," *Nat. Nanotechnol.* **7**(7), 472–478 (2012).
34. J. C. Song et al., "Hot carrier transport and photocurrent response in graphene," *Nano Lett.* **11**(11), 4688–4692 (2011).
35. N. M. Gabor et al., "Hot carrier-assisted intrinsic photoresponse in graphene," *Science* **334**(6056), 648–652 (2011).
36. X. Cai et al., "Sensitive room-temperature terahertz detection via the photothermoelectric effect in graphene," *Nat. Nanotechnol.* **9**(10), 814–819 (2014).

Biographies of the authors are not available.